Structural and Electrochemical Characterization of the Spinel $LiCr_xMn_{2-x}O_4$ System

Sung-Jae Hong, Soon-Ho Chang,† and Chul-Hyun Yo*

Department of Chemistry, Yonsei University, Seoul 120-749, Korea
†Electronics and Telecommunications Research Institute, Taejon 305-350, Korea
Received May 29, 1998

We synthesize the spinel lithium manganese oxides of the $LiCr_xMn_{2-x}O_4$ from x=0.00 to 0.70 at 750 °C in air and identifiy them with X-ray crystallography. We determine the crystallinity, the local structure, and the variation of Mn oxidation states due to the substitution of chromium by the Rietveld and X-ray Absorption Spectroscopy (XAS) analyses. The Rietveld analysis reveals the structure of $LiCr_xMn_{2-x}O_4$ adopts cubic spinel phase with space group $Fd\bar{3}m$. The crystallinity of the spinel compounds improves as the amount of Cr increases, which depends upon variation of the oxidation state in Mn and the existence of Mn in tetrahedral (T_d) sites. The Mn ions have a mixed oxidation state between Mn^{3+} and Mn^{4+} ions. The oxidation state of Mn atoms has more Mn^{4+}ions as the x-value increases. Since Mn^{3+} ions have Jahn-Teller distortion, the decrease of the Mn^{3+} ions increases the crystallinity of compounds. A few Mn ions located in T_d site instead of octahedral (O_h) site cause local disorder. The Mn ions in T_d site decrease with the increasing x-value, which is in agreement with results of the XAS analysis. The Mn-O bond length decreases gradually due to the raising Mn-O covalency and the absorption Mn K-edge shifts to higher energy corresponding to a higher oxidation state. We observe the electrochemical properties of the spinel compounds with $Li//LiCr_xMn_{2-x}O_4$ galvanic cells. We obtain the galvanic cell data under a constant current of 265 μA and a voltage range of 3.4 to 5.2V. The capacity loss on repeated charge and discharge decreases in overall voltage range. The first discharge capacities, however, decrease in the range of 3.4 to 4.3V, while the capacities increase in a range of 4.3 to 5.2V, with x-value due to the oxidation/reduction of Cr in addition to those of Mn. Also the plateau at 4.5V, which is responsible for the oxidation/reduction of Mn in T_d site, gradually disappeared.

Introduction

Recently, concerns about the environment and energy shortages have led to the development of new rechargeable battery systems such as Ni-Cd and Ni-MH batteries.[1] They are gradually being replaced, however, by lithium secondary batteries, which have high specific energy and high voltage.[2~7] In particular, the spinel $LiMn_2O_4$ stands out as the most attractive cathode materials or rechargeable lithium batteries in these days.[5,8~11]

$Li//LiMn_2O_4$ cells offer high performance such as a large discharge capacity of about 110-120 mAh/g and a high voltage of about 4V.[12] Also the $Li//LiMn_2O_4$ cell offers economical and environmental advantages compared with other cathode materials. When y-value is $0 \le y \le 1$ in $Li//Li_yMn_2O_4$ cells, the cells discharge at 4V, whereas when $1 < y \le 2$, the cells discharge at 3V.[13,14] The discharge capacity of $Li//LiMn_2O_4$ cells, however, decreases rapidly as the charge and discharge cycle is repeated.[15,16] The decrease may result from the oxidation of electrolytes during charging, the Jahn-Teller effect by non-equilibrium discharging and the disproportional reaction of Mn^{3+} ions to Mn^{2+} and Mn^{4+} ions.[11] Mn ions at the octahedral site of spinel structure have an average 3.5+ oxidation state.[17] The spinel structure of the cubic unit cell has a phase transition to the tetragonal phase due to Jahn-Teller effect by Mn^{3+} ion with d^4 electron configuration.[11,13,18]

If the $Li//Li_yMn_2O_4$ cell is discharged in the equilibrium state, the lithium ion will be intercalated into the skeleton of the Mn_2O_4 at 4V, resulting in a cubic $LiMn_2O_4$ structure. Since electrochemical cells are generally operated in a non-equilibrium state, the surfaces of the $Li_yMn_2O_4$ electrode become $Li_{1+\delta}Mn_2O_4$ at the end of discharge, whereas the bulk of the electrode becomes $Li_{1-\delta}Mn_2O_4$. Therefore the oxidation state of the surface falls bellow 3.5+ and that of the bulk rises above 3.5+, which cause uneven elongation along z-axis due to Jahn-Teller effect between surface and bulk.

Although tetragonal and cubic phases coexist in surface and bulk, the Jahn-Teller effect of the surface is larger than that of the bulk. While the charge and discharge are repeated, the surface of the $LiMn_2O_4$ electrode becomes dendrite and the efficiency of the electrode decreases. The spinel compound structures such as Jahn-Teller distortion, the probability of inverse spinel phase, and the spinel defect may be closely associated with the electrochemical properties. The substitution of Cr^{3+} for Mn^{3+} will decrease the Jahn-Teller effect, so that the distortion of the spinel structure can decrease.

The structural change of the spinel compound has been studied with XAS in addition to the Rietveld analysis, followed by the study of the electrochemical performance. X-ray absorption spectroscopy is the most powerful method for local structure analysis such as bond length, electronic environment, oxidation state, coordination number etc.[19,20] While extended X-ray absorption fine structure (EXAFS) spectroscopic analysis provides very accurate information on first-shell metal-ligand distance, it determines the site

geometry with less accuracy. Complementary information can be obtained, however, by X-ray absorption near edge structure (XANES) spectroscopy.

In this study, the substitution effects of Cr for Mn in the spinel system with respect to the structures and their electrochemical properties are investigated.

Experimental Section

The $LiCr_xMn_{2-x}O_4(0.0\leq x\leq 0.7)$ spinel compounds were prepared from the stoichiometric mixture of Li_2CO_3, Cr_2O_3, and chemically prepared λ-MnO_2. The mixture, finely ground, is burned at 600 °C for 5 hours and then sintered at 750 °C in air for 48 hours with intermediate grinding and pelleting. All of the compounds are analyzed by the Rietveld refinement of X-ray crystallographic data measured with Mac-science 18 kW X-ray diffractometer at 0.02 deg/sec scan rate. The DBWS-9006pc software is used for the rietveld calculation from cerius 2 program.

X-ray absorption spectra were recorded on BL3C1 station under ring conditions of 2 GeV and 100-150 mA at the Pohang Light Source (PLS). The radiation is monochromatized using a Si(111) double crystal monochromator. The XANES spectra were recorded from *ca.* 200 eV before absorption edge to 100 eV after the edge in 0.2 eV steps. The EXAFS spectra were also collected to *ca*. 1000 eV after the edge in 0.02 k steps. The calibration was carried out with λ-MnO_2 and Cr-metal foil and then the spectra of Mn K-edge (6539 eV) and Cr K-edge (5759 eV) in transmission mode, were recorded using N_2-filled ion chamber at ambient temperature and pressure. All EXAFS spectra were analyzed with UWXAFS 3.0 and FEFF 6.01 code, which calculate the theoretical XAFS spectra by *ab initio* multiple scattering approach.

The electrochemical properties of spinel compounds were observed with a galvanic half cell composed of a Li-metal anode, a $LiCr_xMn_{2-x}O_4$ cathode, and with 50% compressed acethylene black(AB) added for improved conductivity, and PTFE (polytetra-fluoroethylene) as binder. $LiPF_6$ in organic solvent composed of EC (ethylene carbonate) and DMC (dimethyl carbonate) with a volume ratio of 2:1 was used as electrolytes. The MacPile Galvanostatic system was also used for galvanic measurement. The galvanic data are obtained under constant current of 265 μA between 3.4V and 5.2V. The cycle performance on repeated charge and discharge was independently investigated in voltage ranges of 3.4V to 4.3V and of 4.3V to 5.2V.

Results and Discussion

X-ray crystallographic analysis The powder diffraction patterns of the $LiCr_xMn_{2-x}O_4$ system can be assigned to cubic spinel phase with space group *Fd*3*m*. Figure 1(a) shows XRD pattern carried out the Rietveld refinement. The lattice parameter decreases gradually as substitution of Cr for Mn increases as listed in Table 1, which can be explained by two factors. The first factor is due to the crystal radii, and

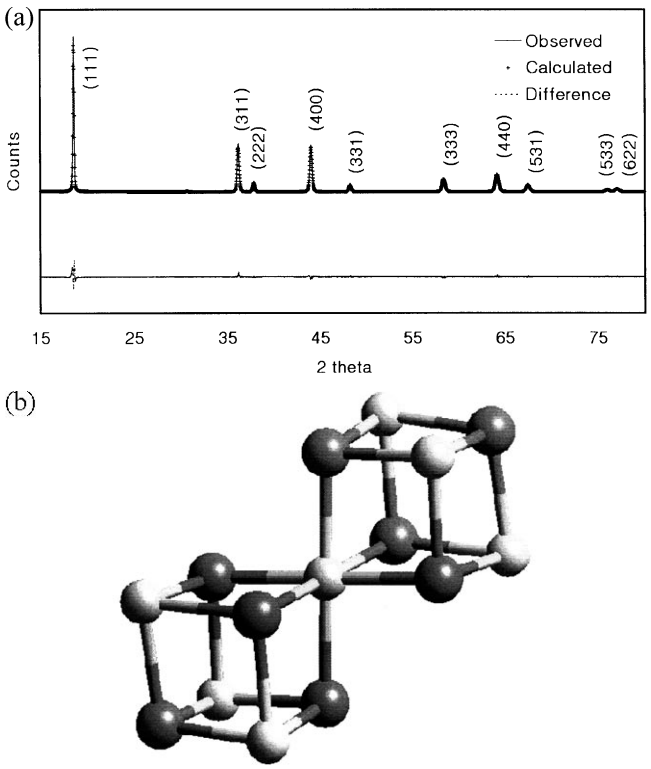

Figure 1. Rietveld fitting for XRD patterns of the $LiCr_xMn_{2-x}O_4$ system (a) and distorted octahedral site in spinel structure (b).

the other is the oxidation state and Jahn-Teller effect. Shannon and Prewitt report that the crystal radii of Mn^{3+} ions are 0.785 Å in high spin and 0.72 Å in low spin, and those of Mn^{4+} and Cr^{3+} ions are 0.67 Å and 0.755 Å, respectively.[21] Therefore, the Cr^{3+} ions can be dominantly substituted for high-spin Mn^{3+} ions instead of the low spin Mn^{3+} or Mn^{4+} ion.

High-spin Mn^{3+} ion has $t_{2g}^3e_g^1$ spin state at the octahedral site which has an elongation on the z-axis according to Jahn-Teller effect. Since the substitution of Cr^{3+} ions for Mn^{3+} ions reduces the elongation on the z-axis, the average bond length of Mn-O decreases slightly. In addition, the mean oxidation state of Mn for non-substituted spinel compound shifts from 3.5+ to 4+ as Cr^{3+} ions increase in $LiCr_xMn_{2-x}O_4$. The higher oxidation state reduces Mn-O bond length and decreases the unit cell parameter. As a result of the Rietveld analysis, reliable R-factor decreases gradually, which means indirectly the improved crystallinity of compounds as listed in Table 1.[22] Since the spinel compounds may have mixed Mn valance, Jahn-Teller distortion, and unusual Mn in the tetrahedral site, it cannot be well ordered.

Figure 1(b) shows that the spinel octahedral sites are distorted. The O-Mn-O bond angle is about 96° to opened tunnel whereas 84° to closed cubic. The determination of atom posi tion by the Rietveld refinement is not accurate because of the averaging of the position on different atoms such as substituted atoms, but it can be accepted roughly. The lower Jahn-Teller distortion and the removal of Mn in the tetrahedral agrees with the result of Rietveld analysis. It will be

Table 1. The cell parameter and Rietveld analysis data of the $LiCr_xMn_{2-x}O_4$ system

Composition(x)	Cell parameter a(Å)	Reliable R-factor			Goodness of fit
		R_e	R_p	R_{wp}	
x=0.00	8.236	6.35	12.04	16.81	2.65
x=0.12	8.230	6.38	10.64	14.96	2.34
x=0.25	8.216	5.84	10.19	14.64	2.51
x=0.37	8.207	6.26	9.00	13.32	2.13
x=0.50	8.196	6.23	9.20	13.23	2.12
x=0.62	8.194	6.13	8.70	12.91	2.11

explained later in association with X-ray absorption spectra analysis and electrochemical performance.

XAS analysis XAS spectra obtained at BL3C1 compartment of Pohang Light Source (PLS) were analyzed in EXAFS and XANES regions. Figure 2 shows Fourier transformed EXAFS spectra of the fitting data in range of 1Å≤r≤3Å and Fourier transformed experimental data (a) and k^3-weighted inverse Fourier transformed data (b). The two peaks with high intensity correspond to first ligating oxygen and the second neighbor octahedral site metal ion. The bond length between atoms, Debye-Wallar factor, and EXAFS Fitting parameter of the $LiCr_xMn_{2-x}O_4$ system are listed in Table 2. Mn-O bond lengths shorten from 1.92(6) Å to 1.90(6) Å, according to the x value, but Cr-O bond lengths are all the same, or about 1.99(7) Å.

Mixed valence Mn K-edge analysis in the EXAFS spectra does not give a good r-factor between 2% and 3%, whereas the Cr K-edge analysis gives a good r-factor within 1%. This may result from the mixed valency Mn oxidation states. The first coordination number of Mn and Cr is 6 and thus both Mn and Cr are located in the octahedral site.

The XANES analysis shows more clearly the change in Mn environments. Mn K-edge XANES spectra have 4 peaks of A, B, C, and D as shown in Figure 3. The C and D peaks of the high intensity correspond to 1s→4p transition. According to selection rule, the transition of $\Delta l=\pm1$ is electric dipole allowed. Therefore, 1s→4p transitions have high transition probability or high intensity.

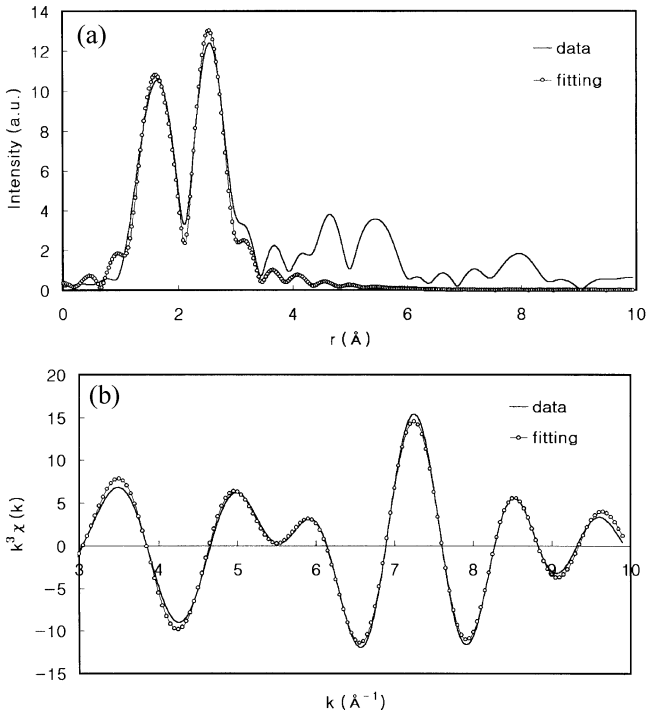

Figure 2. Fourier transformed EXAFS spectra in r-space (a) and inverse Fourier transformed EXAFS spectra in k-space (b) of the $LiCr_xMn_{2-x}O_4$ system.

The metal ion p-orbital of the Mn-O-Mn bond has two bonding components of σ and π. The structure of spinel compounds has a Mn-O-Mn bond angle of about 90° as shown in Figure 1, whose σ component at axes is stronger than π component, with side overlap of π orbitals. Whereas a Metal-O-Metal bond of 180° has a stronger π component than σ component at axes. Since a σ* anti-bonding character is located at higher energy level than the π* by molecular orbital theory, the transition of $1s \rightarrow |1s^1 3d^n 4p\sigma^{*1}>$ occurs at higher absorption energy. Therefore, C and D peaks correspond to $1s \rightarrow |1s^1 3d^n 4p\pi^1>$ and $1s \rightarrow |1s^1 3d^n 4p\sigma^1>$ transitions, respectively, in XANES spectra. While the perovskite compound (ABO_3)[23] of the 180° bond angle has more intense C peak, the spinel compound with 90° bond angle has the D peak.

Table 2. The bond-length between atoms, Debye-Waller factor, and EXAFS fitting parameter of the $LiCr_xMn_{2-x}O_4$ system

Composition (x)	Mn-O		Cr-O		Mn-Mn(Cr)		Cr-Mn(Cr)		Fitting r factor	
	Bond length (Å)	σ^2	Bond length (Å)	σ^2	Bond length (Å)	σ^2	Bond length (Å)	σ^2	Mn K-edge	Cr K-edge
x=0.00	1.926	0.00598	-	-	2.902	0.00366	-	-	0.2845	-
x=0.12	1.921	0.00626	-	-	2.903	0.00382	-	-	0.01735	-
x=0.25	1.917	0.00618	1.998	0.00641	2.886	0.00382	2.881	0.00414	0.02020	0.00923
x=0.37	1.916	0.00618	1.996	0.00545	2.884	0.00377	2.880	0.00353	0.02018	0.01110
x=0.50	1.913	0.00359	1.996	0.00688	2.878	0.00253	2.864	0.00436	0.02929	0.01003
x=0.62	1.906	0.00626	1.998	0.00578	2.877	0.00312	2.860	0.00372	0.01804	0.00993

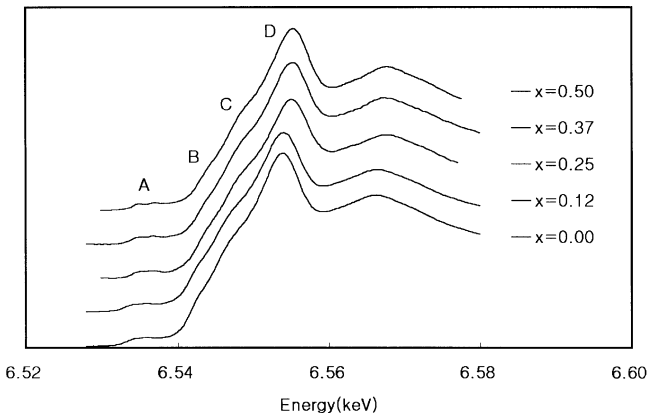

Figure 3. Mn K-edge XANES spectra of the $LiCr_xMn_{2-x}O_4$ system.

The pre-edge A peak corresponds to 1s → 3d transition, which is formally electric dipole forbidden. Experimentally, the electric quadrupole nature of the 1s → 3d pre-edge feature in D_{4h} $CuCl_4^{2-}$ was demonstrated by Hahn *et al.*[24] with an analysis of the angular dependence of 1s → 3d transition intensity, using polarized synchrotron radiation and oriented single crystals. The p-orbital mixing into 3d orbitals can also contribute to pre-edge intensity, which has much higher intensity than the electric quadrupole allowed transition. Since the distorted octahedral site as shown in Figure 1(b) may feel non-zero net electric field, an electric quadrupole transition can occur.

A peak splits into A' and A" subpeaks as the x value increases as shown in Figure 3. This can be shown, obviously, in the second derivatives of raw spectrum as shown in Figure 4(a). The relative intensity and peak positions of A' and A" fitted with Lorentzian function are listed in Table 3. The A" peak intensity decreases gradually and the energy difference between A' and A" increases slightly with the x value. The 3d orbital in an octahedral site splits t_{2g} and e_g orbitals corresponding to A' and A" peaks, respectively.[25] The A" intensity relative to A' decreases gradually with the increasing x value, which means the increase in covalency in Mn-O bond. The increase in covalency in Mn-O bond reduces the 3d orbital component of Mn and then induces lower transition probability to the 3d orbital or lower intensity of the pre-edge feature.

Since e_g orbitals are distributed to axes, they are more affected by covalency than t_{2g} orbitals. Therefore, A" peak intensity corresponding to the transition to e_g orbital decreases more rapidly. This shows why Mn-O bond lengths gradually shorten in the EXAFS analysis. As Mn-O bond lengths decrease, 10Dq between t_{2g} and e_g orbitals in the octahedral site increases from 2.1 eV to 2.5 eV. Cr K-edge XANES spectra have no subpeaks, which can be differentiated in A. Cr-O bond has weaker covalency than Mn-O and thus its bond length is longer than that of Mn-O bond as shown in EXAFS results. The small splitting of 10Dq contributes to overlap subpeaks, and then it appears to be only one peak as shown in Figure 4(b).

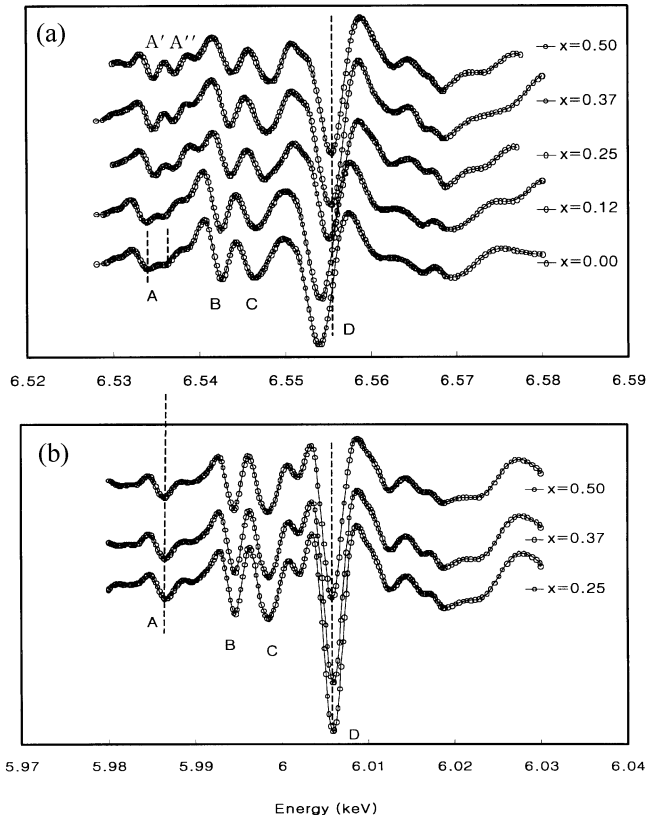

Figure 4. The second derivatives of Mn K-edge XANES spectra (a) and Cr K-edge XANES spectra (b) for the $LiCr_xMn_{2-x}O_4$ system.

The B Peak corresponds to the shake-down process in which 1s → 4p transition with ligand → 3d electron transition or ligand to metal charge transfer (LMCT) occurs at the same time as total 1s → $|1s^13d^{n+1}\underline{L}^{-1}4p^1>$ transition. Since the binding energy decreases due to the core-hole screening effect in Mn by an electron transferred in ligand, the transition in shake-down process occurs at lower energy.[26]

The Mn K-edge XANES spectra shift to high energy with the increasing x value due to the increasing oxidation state of Mn. The Cr K-edge XANES spectra do not shift with the amount of Cr since the Cr located in the octahedral site has a coordination number of 6 without the oxidation state variation.

Electrochemical performance. The capacity of Li// $LiCr_xMn_{2-x}O_4$ has been observed in a range between 3.4V

Table 3. Peak fitting result with Lorentzian function of the $LiCr_xMn_{2-x}O_4$ system

Composition	Relative intensity		$\Delta E(E_{A"}-E_{A'})$
	A'	A"	
0.00	1.00	1.08	2.1 eV
0.12	1.00	0.87	2.1 eV
0.25	1.00	0.86	2.2 eV
0.37	1.00	0.76	2.4 eV
0.50	1.00	0.75	2.5 eV

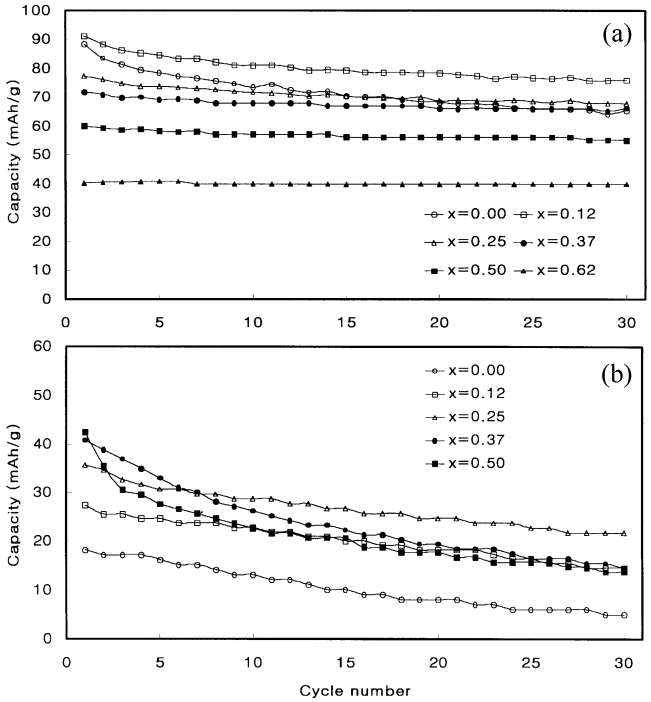

Figure 5. The capacities of the $Li/LiCr_xMn_{2-x}O_4$ cells in ranges of 3.2V to 4.3V (a) and of 4.3V to 5.2V (b).

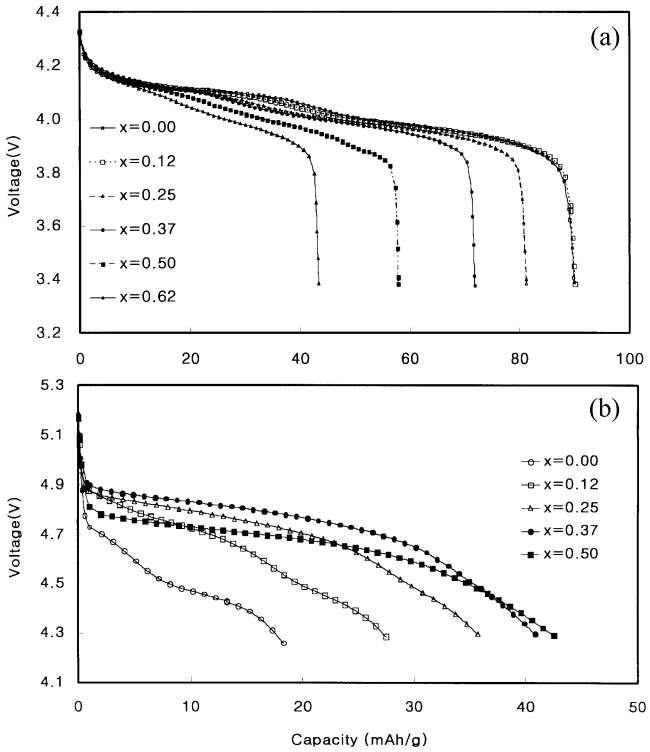

Figure 6. The capacity losses on the first 30 cycles of the $LiCr_xMn_{2-x}O_4$ system in the range of 3.2V to 4.3V and of 4.3V to 5.2V (b).

and 5.2V. The Mn ion oxidized at 3.4-4.3V is usually located in octahedral site, but that oxidized at 4.3-5.2V is surrounded by a different electronic and structural environment. Therefore, the capacity and voltage variations are independently measured in ranges of 3.4-4.3V and 4.3-5.2V.

Figure 5(a) shows that the first discharge capacity in the range of 3.4V to 4.3V decreases as the amount of Cr increases in agreement with other results.[27] The capacity of the x=0.12 is, however, almost the same with about 90 mAh/g of non-substituted $LiMn_2O_4$ in the range of 3.4V to 4.3V. Non-substituted spinel manganese oxide deintercalate $0.8Li^+$ per formula unit during charge and intercalate $0.6Li^+$ per formula unit during discharge. Since deintercalating 1 mole Li^+ corresponds to 1 mole Mn^{3+} oxidation, $0.2Mn^{3+}$ per 1 mole $LiMn_2O_4$ does not react in the first charge/ discharge. The composition of x=0.12 have no affect at all in charge/discharge and the capacity of $Li//LiCr_{0.12}Mn_{1.88}O_4$ is preserv-ed. The composition of x≥0.25, however, decreases capacities step by step due to the decrease in reacted Mn^{3+} ions.

Although the capacity in the range of 4.3V to 5.2V increases with the x value, it is saturated in the x≥0.37 as shown in Figure 5(b). The composition of x=0.62 has no capacity in this voltage range due to the large voltage drop. The plateau at 4.5V in non-substituted spinel manganese oxide disappears gradually and that at about 5V appears with the increasing x value.

Tarascone *et al.*[28] reported that the 4.5V plateau in $LiMn_2O_4$ is associated with oxidation of Mn in the tetrahedral site. The plateau does not, however, show any evidence of the existence of Mn in the tetrahedral site. A few Mn may unfavorably exist as the initial synthetic condition in the tetrahedral site of the spinel structure within the error range of XAS and the Rietveld analyses. Therefore, electrochemical methods may be complementary with spectroscopic methods. The reduction of the 4.5V plateau indicates the removal of Mn in the tetrahedral site, which is indirectly expected with the Rietveld analysis.

The origin of 5V plateau has not been defined clearly. It has been reported that the 5V plateau owes to $Mn^{4+} \rightleftarrows Mn^{5+}$ oxidation/reduction or the removal of the octahedral site Li in spinel structure.[17,29] The structural stabilization is verified with XAS and the Rietveld analyses as the chromium substitution reveals more probable Mn reaction than the removal of Li in the octahedral site. The Cr^{3+} ions oxidation to Cr^{4+} ions at about 5V *vs* Li electrode has been reported recently.[30] The Mn^{4+} and Mn^{5+} ions have the same electron configuration of d^3 and d^2 as Cr^{3+} and Cr^{4+} ions, respectively. Therefore, the origin of the nearly 5V plateau might be the $Mn^{4+} \rightleftarrows Mn^{5+}$ reaction. As the Cr amount increases, the main reaction becomes Cr oxidation/reduction instead of Mn oxidation/reduction and thus the capacity increases due to the Cr reaction.

The discharge voltage with the Cr substitution rises exponentially untill the x=0.37 and then a large voltage drop occurs in the x≥0.5. The composition of x=0.5 shows lower voltage than in the x=0.37 and x>0.5 and does not show the discharge voltage in 4.3-5.2V. The more the resistance on Li diffusion increases with the x-value, the larger the discharge voltage drop.

The cycle performance improves both high and low voltage ranges. Non-substituted spinel manganese oxide has about a 74% capacity in the range of 3.2V to 4.3V on the first discharge capacity after 30 cycles. The compositions of x=0.12 and 0.25 have 83% and 87% capacities, respectively. The capacity loss gradually decreases with the increasing x value. Since the first discharge capacity is much less in the case of x≥0.25 relative to the non-substituted compound, the effect of good cycle performance may be canceled.

Only the composition of x=0.12 shows attractive results as shown in Figure 6(a). Since the increase of Mn-O covalency verified by XANES analysis preserves more effectively the spinel skeleton on Li intercalation/deintercalation, the capacity loss on charge/discharge cycles decreases. Figure 6(b) shows different cycle performance in the range of 4.3V to 5.2V. The performance in the case of x=0.12 and x=0.25 is better than the non-substituted compound as observed at in low voltage, but the capacity loss on cycle increases rapidly above x=0.37.

The observation of reversible charge/discharge cycle suggests that the capacities in the high-voltage range are associated with $Mn^{4+} \rightleftarrows Mn^{5+}$ and $Cr^{3+} \rightleftarrows Cr^{4+}$ irrespective of the removal of Li in the octahedral site. Since the reversible intercalation/deintercalation reaction of Li in the octahedral site is unfavorable in thermodynamics, the oxidations of Mn and Cr ions may result in the high-voltage capacity. The large resistance on Li diffusion in Cr oxidation/reduction shows poor cycle performance above x=0.37.

Conclusion

Improvement of crystallinity has been confirmed with the Rietveld analysis showing that an R-factor decreases more rapidly as the x-value increases. The XAS study confirms that Mn-O bond length becomes shorter and thus Mn-O bond covalency increases gradually while Cr-O bond length does not change as the amount of Cr increases. The structural stabilization of spinel $LiCr_xMn_{2-x}O_4$ results from the raise in Mn-O covalency, the removal of Mn in the tetrahedral site, and the reduced Jahn-Teller effect. This causes the good cycle performance in comparison with non-substituted spinel manganese oxides in the range of 3.2V to 4.3V and a lower 4.5V plateau due to Mn in the tetrahedral site. The substitution of Cr for Mn increases high voltage capacity, which results from Mn^{4+}/Mn^{5+} oxidation/reduction in addition to Cr^{3+}/Cr^{4+} oxidation/reduction.

The cycle performance is improved in the range of 3.2V to 4.3V due to structural stabilization. The capacity loss on cycle in the range of 4.3V to 5.2V decreases from x=0.00 to x=0.25, but it increases above x≥0.37.

Acknowledgement. The present study was supported by project No. 96-0501-0601-3 of the Korean Science and Engineering Foundation in 1996 and therefore we express our appreciation to the authorities concerned.

References

1. Masaki, Y. "Lithium ion Batteries" p 171, Department of Applied Chemistry, Saga university, **1996**.
2. Imanishi, N. *J. Electrochem. Soc.* **1990**, *140*, 315.
3. Nagaura, T.; Tozawa, K. *Prog. Batt. Solar Cells* **1990**, *9*, 209.
4. Whittingham, M. S. *Prog. Solid State Chem.* **1978**, *12*, 41.
5. Thackeray, M. M. *J. Electrochem. Soc.* **1995**, *142*, 2558.
6. Sewai, K.; Iwakoshi, Y.; Ohzuku, T. *Solid State Ionics* **1994**, *69*, 273.
7. Brandt, K. *Solid State Ionics* **1994**, *69*, 173.
8. Koksbang, R.; Barker, J. *Solid State Ionics* **1996**, *84*, 1.
9. Ohzuku, T. *J. Electrochem. Soc.* **1990**, *3*, 137.
10. Gao, Yuan; Dahn, J. R. *J. Electrochem. Soc.* **1996**, *143*, 100.
11. Tarascon, J. M.; Wang, E.; Shokoohi, F.K. *J. Electrochem. Soc.* **1991**, *138*, 2859.
12. Ohzuku, T.; Ueda, A. *Solid State Ionics* **1994**, *69*, 201.
13. Thackeray, M. M.; David, W. I. F.; Bruce, D. G.; Goodenough, J. B. *Mat. Res. Bull.* **1983**, *18*, 461.
14. Thackeray, M. M.; Johnson, P. J.; L A de Picciotto *Mat. Res. Bull.* **1984**, *19*, 179.
15. Summow, R. J.; De Kock, A.; Thackeray, M. M. *Solid state ionics* **1994**, *69*, 59.
16. Macklin, W. J.; Neat, R. J.; Powell, R. J. *Journal of Power Sources* **1991**, *34*, 39.
17. Bates, J. B.; Lubben, D.; Dudney, N. J.; Hart, F. X. *J. Electrochem. Soc.* **1995**, *142*, L149.
18. Ohzuku, T.; Kitagawa, M.; Hirai, T. *J. Electrochem. Soc.* **1990**, *137*, 769.
19. Lee, P. A.; Pendry, J. B. *Physical Review B* **1975**, *11(8)*, 2795.
20. Teo, Boon K. *EXAFS: Basic Principles and Data Analysis*; Springer-Verlag: Berlin, **1986**; p 32.
21. Shannon, R. D.; Prewitt, C. T. *Acta Crystallography*, **1972**, *A32*, 751.
22. Young, R. A. *The Rietveld Method*; Oxford University Press Inc.: New York, **1993**; p 3.
23. Ryu, K. H. *Synthesis, Spectroscopic Analysis, and Characterization of the Perovskite and Spinel Ferrites*; Yonsei University: Seoul, **1996**; p 70.
24. Hahn, J. E.; Scott, R. A.; Hodgson, K. O.; Doniach, S.; Desjardins, S. R.; Solomon, E. I. *Chem. Phys. Lett.* **1982**, *88*, 595.
25. Westre, T. E.; Kennepohl, P.; Dewitt, J. G.; Hodgson, K. O.; Solomon, E. I. *J. Am. Chem. Soc.* **1997**, *119*, 6297.
26. Iwasawa, Y. *X-ray absorption fine structure for catalysts and surfaces*; World Scientific Publishing Co.: Singapore, **1996**; p 73.
27. Sigala, C.; Guyamard, D.; Verbaere, A.; Piffard, Y.; Tournoux, M. *Solid State Ionics* **1995**, *81*, 167.
28. Guyomard, D.; Tarascon, J. M. *Solid State Ionics* **1994**, *69*, 222.
29. Sigala, C.; Verbaere, A.; Mansot, J. L.; Guyamard, D.; Piffard, Y.; Tournoux, M. *Journal of Solid State Chemistry* **1997**, *132(2)*, 372.
30. Tarascon, J. M.; Mckinnon, W. R.; Coowar, F.; Bowmer, T. N.; Amatucci, G.; Guyomard, D. *J. Electrochemical Soc.* **1994**, *141*, 1421.